Vaporization and Collision Modeling of Liquid Fuel Sprays in a Co-axial Fuel and Air Pre-mixer

Xin Gu[1*], Saptashi Basu[2], Ranganathan Kumar[3]
[1,3]Department of Mechanical Materials and Aerospace Engineering
University of Central Florida, Orlando FL 32816
[2]Department of Mechanical Engineering, Indian Institute of Science, Bangalore 560012, India
xgu@knights.ucf.edu, sbasu@mecheng.iisc.ernet.in and Ranganathan.Kumar@ucf.edu

Abstract

Droplet collision occurs frequently in regions where the droplet number density is high. Even for lean pre-mixed pre-vaporized (LPP) liquid sprays, the collision effects can be very high on the droplet size distributions, which will in turn affect the droplet vaporization process. Hence, in conjunction with vaporization modeling, collision modeling for such spray systems is also essential. The standard O'Rourke's collision model, usually implemented in CFD codes, tends to generate unphysical numerical artifact when simulations are performed on Cartesian grid and the results are not grid independent. Thus, a new collision modeling approach based on no-time-counter method (NTC) proposed by Schmidt and Rutland is implemented to replace O'Rourke's collision algorithm to solve a spray injection problem in a cylindrical coflow premixer. The so called "four-leaf clover" numerical artifacts are eliminated by the new collision algorithm. Next, the dispersion and vaporization processes for liquid fuel sprays are simulated in a coflow premixer. Two liquid fuels under investigation are jet-A and Rapeseed Methyl Esters (RME). Results show very good grid independence. At relatively low spray cone angle and injection velocity, we found that the collision effect on the average droplet size and the vaporization performance are very high due to relatively high coalescence rate induced by droplet collisions. We also found that the vaporization performance and the level of homogeneity of fuel-air mixture can be significantly improved when the dispersion level is high, which can be achieved by increasing the spray cone angle and injection velocity.

Introduction

Lean Premixed and Pre-vaporized (LPP) combustion is a proven alternative technology to achieve better performance than traditional diffusion mode of combustion. For LPP gas turbine that operates on liquid fuels, a pre-vaporization chamber, called premixer in which the liquid fuels are sprayed into hot air-stream is needed prior to combustion. Therefore, clear understanding of the dynamics of the fuel spray and the corresponding vaporization process in the premixer is very important.

Different liquid fuels normally have very different transport properties which will result in different vaporization characteristics. This could affect the design of the premixing duct, such as the duct length, contraction/expansion ratio, and different spray control parameters, such as spray velocity and spray cone angle. Both single droplet [1-6] and turbulent spray [7-8] vaporization process have been studied extensively in the literature. Abramzon and Sirignano [5] developed a two-dimensional transient droplet vaporization model based on the assumption of Hill's vortex in the liquid phase. Their model included the effects of variable thermophysical properties, non-unitary Lewis number, effects of Stefan flow, effects of droplet internal circulation and transient liquid heating with vaporization. The details of the mathematical model are given by Sirignano [9]. This vaporization model has been shown to be very accurate for predicting single droplet vaporization [5,10]. Torres et al. [11] developed an efficient one-dimensional multi-component fuel vaporization model and implemented it into a multi-dimensional CFD code: KIVA-3V. Their efficient computational algorithm showed very promising computational speed for three-dimensional spray simulations while capturing the droplet vaporization rate which compared quite well to the experiment.

Barata [8] presented a numerical study on evaporating biofuel droplets injected into a turbulent crossflow of air. Their model did not consider any heat and mass transfer inside each individual droplet, although the temperature and species composition gradients inside the droplet are found to play a very significant role on the droplet vaporization rate during the stage of transient droplet heating [5]. Gu et al. [12] systematically studied the liquid fuel vaporization process in a crossflow premixer for both cold injections and pre-heated injections and showed that the influence of transient droplet heating on the droplet vaporization rate is very important.

For any solid cone sprays, the number density of droplets could be very high for some regions where the collisions between droplets occur very frequently, which will in turn have high impact on the droplet size

* Corresponding author: Ranganathan.Kumar@ucf.edu

distribution [13]. Thus, along with vaporization modeling, collision modeling is desirable in spray simulation in order to capture the droplet size distributions accurately. Droplet collision modeling within a spray is a very challenging problem [14] since collision is a complex physical process, which could lead to different outcomes. In general, the outcomes maybe bouncing, stable coalescence, reflexive separation, stretching separation and shattering depending on the operating conditions [15,16].

Typical liquid spray systems usually involve millions of droplets. Thus, stochastic collision modeling is among the most popular approaches used for spray simulations. O'Rourke's droplet collision algorithm [13] is one of the most widely used model in multi-dimensional spray simulations. However, their collision model cannot achieve grid-independent results due to the use of the gas phase mesh for collision computations. Subramaniam and O'Rourke [17] did a systematic study on the numerical convergence of KIVA-3 code, and found that grid-independent results cannot be achieved for diesel injection problems. Schmidt and Rutland have also reported that the collision results from KIVA can be highly grid-dependent [18]. They also proposed a new modeling method based on no-time-counter (NTC) method [19], where a separate dynamic collision mesh is used for spray collision calculations and their approach indeed yields grid-independent results.

In the current proposed work, we have implemented the NTC collision algorithm into KIVA-4 code and subsequently applied it to spray simulations for coaxial flow injection methods for a typical cylindrical premixer. It should be noted that the collision modeling is not restricted to cylindrical premixer and can be applied with appropriate modifications to rectangular geometry as well.

Numerical Methods

Lagrangian-Eulerian approach is implemented in KIVA-4 code, where the liquid phase is treated as a discrete second phase with mass, momentum and energy coupled (two-way) to the continuous gas phase. Thus, the species mass transport equation, momentum equation and energy equation for the continuous gas phase are solved with extra source terms originating from the discrete droplet phase. The detailed descriptions of those source terms can be found in KIVA-II manual [20] and also in Gu et al [12].

For the cases considered in this paper, the droplet Reynolds number is very small [O(10) initially], and hence the assumption of using only Spalding mass transfer number is generally valid [2].

$$C_D = \frac{24}{\mathrm{Re}_d(1+B_d)} \tag{1}$$

with droplet Reynolds number defined as:

$$\mathrm{Re}_d = \frac{2\rho_g \left|\mathbf{u}+\mathbf{u}'-\mathbf{u}_d\right| r_d}{\mu_g(\hat{T})} \tag{2}$$

where μ_g is the dynamic viscosity of air, which is calculated at the average film temperature defined by $\hat{T} = (T_g + 2T_s)/3$.

Comparing with the original drag model implemented in KIVA, this drag model incorporated the Stefan flow correction for regimes where strong evaporation will reduce the drag coefficient for the vaporizing droplet as proposed by Renksizbulut and Yuen [21]. This drag model is valid for low droplet Reynolds number in the range of $\mathrm{Re_d}$<30 [9]. For current co-axial flow applications, the droplet Reynolds number is very small [O(10) initially], and hence this modified drag model is applicable.

Experimental data indicate that shattering due to collision will not occur if $\mathrm{We_{col}}$<40 [13]. However, at high collision Weber number, fragmentation of droplets during binary collisions can be very important. Georjon and Reitz [22] implemented a simplified drop-shattering collision model into KIVA-II code for collisions when $\mathrm{We_{col}}$>100 based on Rayleigh linear jet breakup theory. For all the premixer simulation cases studied in this paper, the collision Weber numbers were directly recorded and most of the values were found to be less than 40. So the current modeling of collision outcomes as implemented in KIVA-4 would still be valid. For extremely high speed injection with Weber number in the range of 100, the current model will overpredict the droplet size due to the absence of the shattering mechanism in the implemented code.

NTC algorithm is briefly discussed here and details of the model could be found in [18,19].

For each collision cell, the number of candidate pairs, $\mathrm{M_{cand}}$, is randomly chosen among all possible pairs of parcels. And a collision will take place between parcel i and parcel j if the normalized probability is larger than the random deviate, XX in the interval of [0,1):

$$\frac{n_j A_{i,j} u_{i,j}}{(nAu)_{\max}} > XX \tag{3}$$

Making a proper choice to obtain the value of $(nAu)_{max}$ is very important. Current implementation loops over all the parcels in each collision cell to find out the maximum value of nAu, and assigns a coefficient to obtain $(nAu)_{max}$: $(nAu)_{max}$=a*Max(nAu), with a>1. Although this approach requires one additional do-loop in the code which slows down the simulation a little bit, good numerical accuracy is ensured.

However, in order to use NTC collision scheme, the following criteria must be satisfied:

$$M_{cand} < \frac{n_p^2}{2} \tag{4}$$

Since it is not possible that the candidate pairs could exceed the total number of possible pairs, therefore:

$$(nAu)_{\max} < \frac{V_{cell}}{\Delta t} \tag{5}$$

This inequality is a measure of how well the spray is resolved by comparing the swept volume of the colliding parcels to the volume of the collision cell for a specified time step, Δt. Thus, when Δt is very large compared to the actual collision time, this inequality will not be satisfied. Although the satisfaction of this inequality is highly desirable to ensure a well-resolved collision calculation, a safety switch is implemented from the NTC collision calculation to direct single-cell collision (DSCC) for those under-resolved regions. The DSCC scheme is the same as O'Rourke's model except that it takes the advantage of grouping parcels into collision cells.

Results and Discussion

First, results from a simple downward spray are compared between O'Rourke's and NTC collision schemes. It is known that O'Rourke's model may generate severe numerical artifact when the simulation is performed on a Cartesian mesh [19]. For example, Figure 1a shows the so-called "four-leaf clover" numerical artifact when the collision model is turned on for a simple non-evaporating downward spray. This numerical artifact is generated due to the fact that parcels which are 90° apart have the highest relative velocity, resulting in collision with the highest probability. If coalescence occurs for those parcel pairs, the resultant parcel will have a flow direction which is 45° offset from the x-axis or y-axis. This is the reason why the parcel number density becomes lower near the axis, whereas the spray morphology is supposed to be axisymmetric. By turning off the collision model, this four-leaf clover effects would disappear, which can be seen from Figure 1b. This numerical artifact is also not present when the simulation is performed on a polar mesh shown in Figure 1c because the azimuthal direction is better resolved on a polar mesh where the parcels with the highest relative velocities are separated into different cells. When the NTC collision scheme is applied with a separate polar collision mesh, the four-leaf clover artifact is not seen in Figure 1d when the same simulation is performed on a Cartesian mesh.

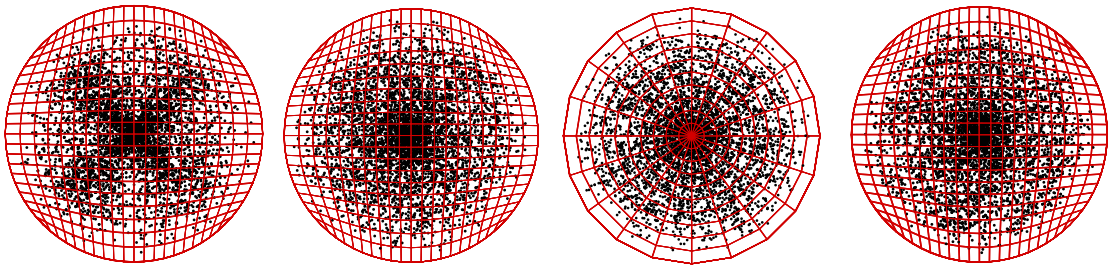

Figure 1 Simulations of a hollow-cone downward spray: a) on a Cartesian mesh using KIVA-4's original collision algorithm b) on a Cartesian mesh with collision model turned off c) on a polar mesh using KIVA-4's original collision algorithm d) on a Cartesian mesh using improved NTC/DSCC collision algorithm

Next, the experimental data of D*ä*if et al. [1] was used to validate the vaporization model. Figure 2 shows comparisons between the simulations and the experiments for single droplets of pure heptane and decane. The result is extracted from one of our numerical experiments [12] and presented here for completeness. The transient change in diameter of both blended and pure decane droplets shows very good agreement with experiments, while the temperature data compares fairly well with experiment with a maximum deviation of 8K.

The corrupting influence from the momentum and drag coupling on the discrete droplet phase is relatively small for larger droplets and this influence is also small even for small droplets when they are away from the nozzle tip [17]. Thus, for all the subsequent pre-mixer simulations, mono-dispersed spray was adopted with an initial droplet size of 80 micron diameter, which is relatively large but is still within the range of practical sprays.

Two types of liquid fuels are investigated here: Jet-A and RME. Jet-A is the primary conventional fuel used in the aviation industry. RME is a biodiesel which can be blended in jet-A. Thus, it is important to study both fuels and compare their vaporization characteristics. Since the fuel vapor pressure is an important parameter for the liquid fuel vaporization process, it is plotted versus temperature for both fuels and is shown in Figure 3. The properties of Jet-A fuel are taken from the tabulated data of KIVA-4 fuel library while RME's properties are

used from reference [10]. It can be seen that vapor pressure is a monotonically increasing function of temperature for both fuels. Vapor pressures for both Jet-A and RME are very low at room temperature, indicating that both of them are non-volatile in nature.

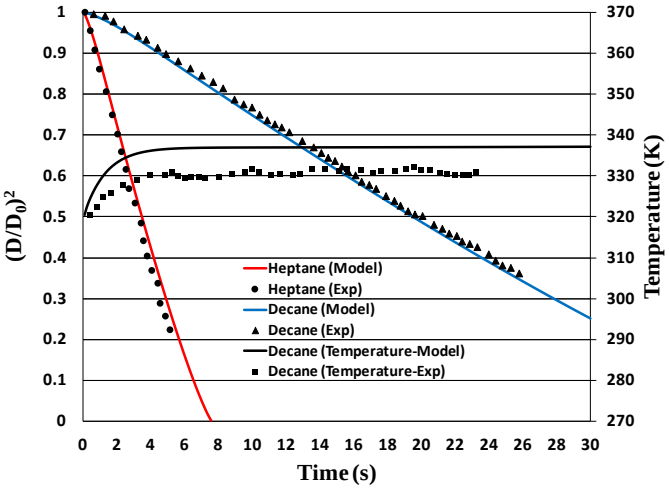

Figure 2 Comparisons between the model and the experiment data for single droplet vaporization

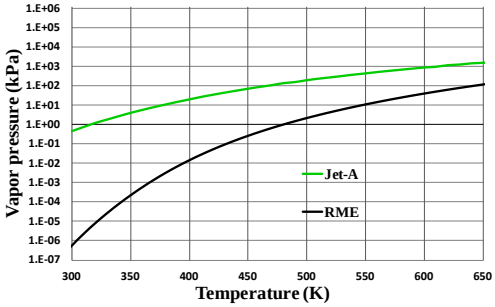

Figure 3 Vapor pressure versus temperature for Jet-A and RME

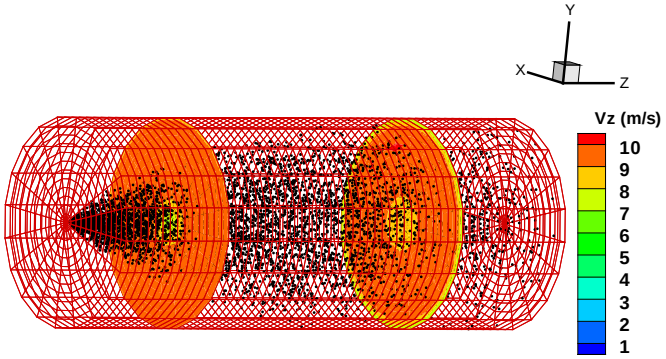

Figure 4 Three-dimensional view of co-axial flow injection with converged gas phase velocity field

The computational domain in Figure 4 represents a typical simplified cylindrical pre-mixer with a length of 300 mm and a radius of 60mm. The pre-mixer has three bounding surfaces with the following set of boundary conditions: the left side is assigned as velocity inlet boundary condition with fixed co-flow velocity and temperature and the right side is pressure outlet boundary condition. The cylindrical surface is assigned law-of-wall boundary conditions. Air is introduced into the pre-mixer at a constant velocity and temperature of 10 m/sec and 800 K respectively. The liquid fuel is injected into the premixer co-axially with the air after the gas phase flow field reached a steady state in about 0.01 s. Figure 4 also shows the contour plot of the gas phase velocity in the co-flow direction at two cross-sectional planes of Z=70 mm and Z=230 mm respectively. The two-way coupling effects can be clearly observed from the velocity contour plot where the velocity near the center of slice decreased due to the inter-phase drag from the discrete droplet phase.

First, we established a baseline set of parameters with a fairly large spray angle of 90° and 3 m/s injection velocity such that the spraying droplets are well dispersed within the premixer while not impacting the wall. All the simulation cases were run at atmospheric pressure. In order to achieve better droplet dispersion and vaporization performance, a high value of turbulent intensity (20% of the mean crossflow kinetic energy) was used for all the simulations reported here. The average number of parcels per collision cell is fixed around 2 since the real collision volume is approximately one third of total volume generated by the polar collision mesh. Thus, the real average number of parcels per collision cell is actually around 6. This is verified by recording both the total number of collision cells that contain at least one pair of parcels and the total number of parcels contained within the simulation volume.

The spray simulations results are presented for both jet-A and RME with the same initial injection temperature of 293 K. Three different mesh resolutions are used. First of all, to show that the results are grid independent, the Sauter-mean-diameters (SMD) of the spray are calculated and plotted versus Z-axis by equally dividing the pre-mixer into 30 zones. The SMD is then normalized by the initial injection SMD, which is D_0. The jet-A spray simulations for three different meshes are presented in Figure 5. Figure 5a shows that the SMD variation

along the z-direction for all three grids. The initial increase of SMD is probably due to the high coalescence rate and low vaporization rate near the injection port where the number density of the droplets is relatively high and the surface temperature of the droplets is relatively low. Meantime, the total number of droplets within each zone is also plotted since it is a good indicator of the spray vaporization performance, and the results for all grids are shown in Figure 5b. The variations of both SMD and total number of droplets along z-axis show very good grid-independence, except that the SMD of coarse grid shows slightly deviation from the other two grids, which is probably because the gas phase is not well resolved. Thus, for the rest of the simulation, the medium mesh resolution is adopted to ensure that the gas phase flow field is well resolved.

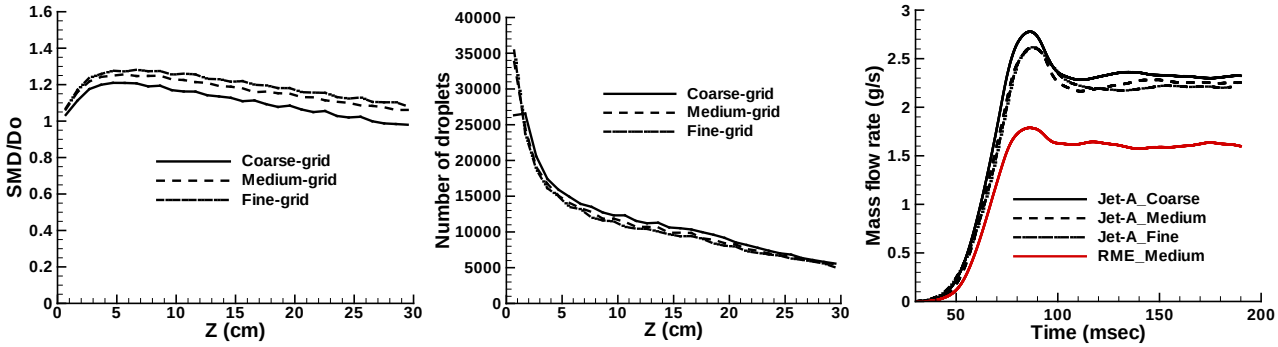

Figure 5 Premixer simulation resolution independence study: a) Normalized SMD vs Z b) total number of droplets vs Z c) Fuel vapor mass flow rate at the premixer exit

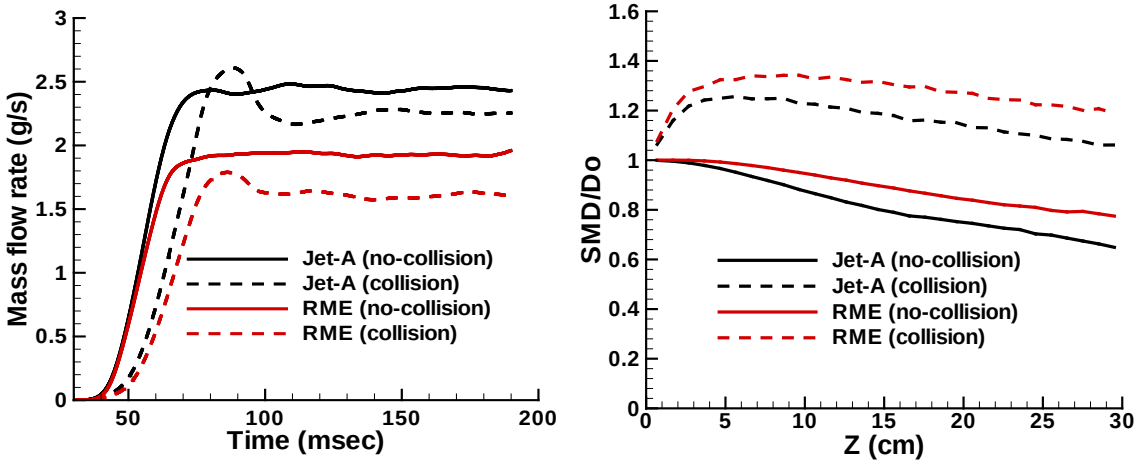

Figure 6 Simulation results of jet-A and RME: a) Fuel vapor mass flow rate at the premixer exit b) normalized SMD plotted along z-axis. Comparisions between simulations without collision model and with collision model for spray cone angle of 90° and injection velocity of 3m/s

Next, quantification of the vaporization performance for each fuel for the current configuration of the pre-mixer is very important. To achieve this, the fuel vapor mass flow rate at the outlet is calculated since it indicates how much percentage of the liquid fuel has been vaporized through the pre-mixer chamber. The jet-A fuel vapor mass flow rates for all grid resolutions are plotted versus simulation time in Figure 5c. Results also show very good grid-independence. The final steady-state jet-A fuel vapor mass flow rate is around 2.2 gram/second for all resolutions. Since the liquid fuel is injected at a rate of 2.7 gram/second, 2.2 gram/second vapor mass flow rate at the outlet indicates that 81.5% of liquid jet-A fuel has been vaporized from the injection point to the outlet of the pre-mixer. The RME fuel vapor mass flow rate (for medium mesh resolution) is also presented in Figure 5c, which shows an average value around 1.6 gram/second, implying that 59.3% of liquid RME has been vaporized through the pre-mixer. There is 22.2% difference in vaporization performance between jet-A and RME, which is obvious from the vapor pressure plot for each fuel as shown in Figure 3. We can see that vapor pressure of jet-A is much higher compared to RME at the same temperature, indicating that jet-A would indeed have a higher vaporization rate.

Furthermore, to show the importance of the collision modeling and its influence in determining the vaporization performance, we turned off the collision model and compared the no-collision simulation results to the results with the collision model activated. From Figure 6a, we can see that the final steady-state jet-A and RME fuel vapor mass flow rates without collision is around 2.4 gram/second and 1.9 gram/second, respectively. This indicated that the vaporization performance is lowered by 7.4% for jet-A and by 11.1% for RME when the collision model is activated. This is primarily due to the coalescence induced by collision leads to surface area de-

struction producing larger droplets that have lower vaporization rate. This can be proved unambiguously from Figure 6b, which shows that the SMD distribution along z-axis for all cases. We can see that the SMD for both fuels will continuously decrease along the z-axis if there is no collision. However in reality SMD for RME increased up to 1.3 times of its original injection size and slowly decreased to 1.2 times of its initial injection size along z-axis when the collision model is activated. Thus, the results show that droplet collisions have high impact on the droplet size distribution which will in turn influence the vaporization performance.

It was shown in the previous section that the vaporization performance for either fuel is not ideal, especially for RME. To explore the possibility of improving the vaporization performance within the current premixer configuration, we tested a series of combinations of spray cone angle and injection velocity since larger spray cone angle and higher injection velocity will improve the dispersion of the injected droplets which will in turn improve the vaporization performance.

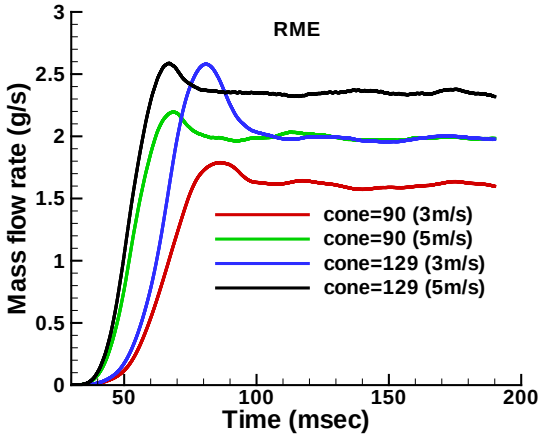

Figure 7 RME vapor mass flow rate at the premixer exit for different combinations of spray cone angle and injection velocity

Several spray cone angles and injection velocity combinations were attempted for the simulation. Beyond 129° and 5 m/s, part of the spray was seen to impact the wall and hence higher combinations were not desired. Including this combination of cone angle and injection velocity, four combinations are presented: 1) 90° and 3 m/s (baseline), 2) 90° and 5 m/s, 3) 129° and 3 m/s and 4) 129° and 5 m/s. Figure 7 shows the RME vapor mass flow rate for all combinations. We can see that the RME vapor mass flow rate exhibits the highest value of 2.3 g/s for 129° of spray angle and 5 m/s of injection velocity, implying that 85.2% of the injected RME fuel has vaporized. Compared to the baseline case, there is 25.9% improvement in vaporization performance for RME. Thus, 129° of spray angle and 5m/s injection velocity serves as an optimum combination to efficiently vaporize the liquid fuels for current premixer configuration.

As done in the previous section, results on the vaporization performance and droplet size distributions are compared between the collision model deactivated and activated (Figure 8). Surprisingly, Figure 8a shows that the vaporization performance is almost identical for both fuels with and without the collision model: jet-A achieved 96.3% in vaporization performance while it is 85.2% for RME. However, the SMD distribution (obtained with collision model) along z-axis as seen in Figure 8b, shows consistently higher value than that obtained without the collision model. Large droplets are expected to have lower vaporization rate, which seems to be contradictory to the identical vaporization performances in Figure 8a. This can be explained as follows: with the collision model activated, the average droplet size could increase due to coalescence; However, the drag equation in conjunction with the droplet acceleration equation (Newton's second law), suggests that the droplet acceleration is inversely proportional to the square of the droplet diameter, i.e., it is smaller for larger droplets. Lower acceleration will result over a longer residence time and vaporization time for the larger droplet in the premixer. Thus, smaller droplet vaporizes faster but also travels faster through the premixer, larger droplet vaporizes slower but also travels slower. Under certain conditions, these two opposing effects can cancel each other in a cumulative sense, leading to approximately similar vaporization performances as obtained without incorporating the collision model. The balance is only achieved in the case of higher spray cone angle and injection velocity, while the baseline results still show lower vaporization performance for results using the collision model. This is because the spray occupies less space at lower spray cone angle and injection velocity, resulting in higher droplet number density, which in turn, promotes droplet collision probability. Figure 6b shows relatively higher SMD along the premixer length for lower spray cone angle and injection velocity.

To quantitatively describe the dispersion level of the spray at different combinations of spray cone angle and injection velocity and show the influence of the collision modeling on the spray dispersions, maximum radial extent of the spray in each zone is calculated along the premixer and normalized by the premixer radius to clearly show how well the spray is dispersed at each condition. RME is used to show these effects in Figure 9. For baseline tests, the collision activated results show relatively higher dispersion level than collision deactivated results. From the previous analysis, we understand that the coalescence rate induced by collision is pretty high

for baseline cases such that the average droplet size is much higher when the collision model is activated. Thus, larger droplets would travel farther in radial direction compared to smaller droplets due to smaller deceleration rates. Therefore, the dispersion level is relatively higher when collision is activated. From Figure 9, it can be seen that the dispersion level for 129° of spray cone angle and 5 m/s of injection velocity is much higher than the baseline tests. This also quantitatively supports our previous analysis where the spray is better dispersed at higher spray cone angle and injection velocity, and improves the vaporization performance significantly.

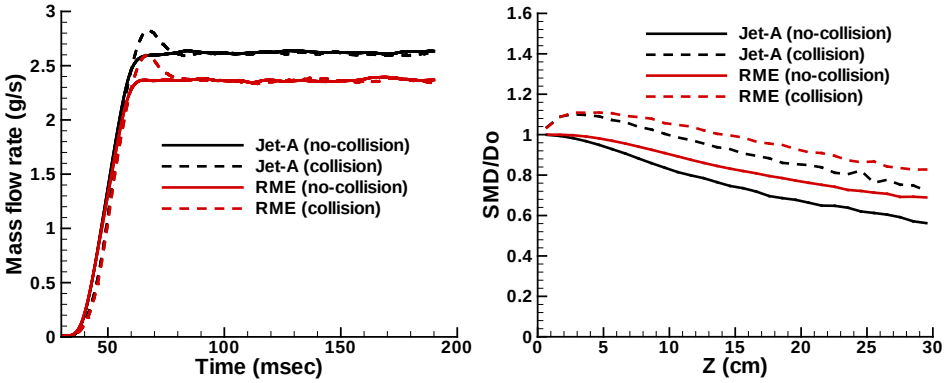

Figure 8 Simulation results of jet-A and RME: a) Fuel vapor mass flow rate at the premixer outlet b) normalized SMD plotted along z-axis. comparisions between simulations without collision model and with collision model for spray cone angle of 129° and injection velocity of 5m/s

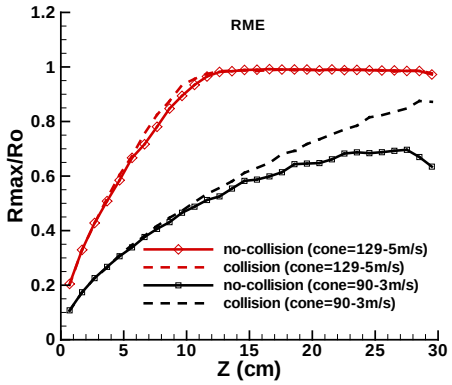

Figure 9 Spray dispersion along z-axis at various conditions

To avoid droplet collision on the walls, swirl is not introduced at the inlet of the pre-mixer. Therefore, in the current configuration, the vapor concentration at the exit is expected to deviate from homogeneity. To quantify the homogeneity of the fuel vapor mass fractions, the so-called "unmixedness" parameter is calculated at the premixer exit [12]. The unmixedness parameter is defined as the standard deviation of the fuel vapor mass fraction divided by the averaged fuel vapor mass fraction within the zone of interest. The ideal value of unmixedness should be zero, meaning perfect homogeneity. For the baseline tests, the values of unmixedness for jet-A and RME are 0.81 and 0.77, respectively. This shows that the extent of inhomogeneity for both fuels is very similar. For the tests at 129° of spray cone angle and 5m/s of injection velocity, the values of unmixedness for jet-A and RME are 0.33 and 0.25, respectively. These low values of unmixedness suggest that the fuel-air mixture is much more homogeneous when the dispersion level of the spray is high.

Summary and Conclusions

In this paper, the numerical code, KIVA-4, has been used with modified collision algorithm based on the NTC/DSCC method. This improved collision algorithm eliminated the "four-leaf clover" numerical artifacts which could appear when using the original collision algorithm implemented in KIVA-4.

The collision algorithm was then subsequently used to simulate the spray and vaporization process in a premixer for both jet-A and RME fuels. The liquid fuels are injected into the premixer co-axially with the air flow. SMD results for a mono-dispersed spray with an initial SMD of 80 μm show very good grid independence for a spray cone angle of 90° and injection velocity of 3 m/s. By comparing the fuel vapor mass flow at the outlet to the liquid fuel injection mass flow rate, it was found that 81.5% of jet-A fuel was vaporized through the premixer and 59.3% for RME. The large difference in vaporization performance between jet-A and RME is due to RME's low vapor pressure. In order to improve the vaporization performance, a series of tests were done for several combinations of spray cone angle and injection velocity. Larger spray cone angle and higher injection velocity expectedly showed improvement in dispersion and vaporization performance. The vaporization perfor-

mance for jet-A for an optimum combination of spray cone angle at 129° and injection velocity at 5 m/s increased to 96.3% and 85.2% for RME. This major improvement in vaporization performance is also partially due to the relatively smaller average droplet diameter which has a higher vaporization rate. Comparisons were also made between collision model deactivated and collision model activated. It was found that the vaporization performance decreased due to high droplet coalescence rate induced by collisions for the baseline tests, while the vaporization performance was not affected at the optimum combination of spray cone angle and injection velocity. For all the above tests, the spray dispersion level was also quantified by calculating the maximum radial extent of the spray in each zone along the premixer. Results show that dispersion level is much higher at larger spray cone angle and injection velocity compared to baseline cases. In order to quantify the homogeneity of the fuel vapor-air mixture, the unmixedness parameter was calculated at the exit of the premixer, which showed that the homogeneity of the fuel-air mixture is significantly improved when the dispersion level of the spray is high.

References

[1] A.Dǎif, M. Bouaziz, X. Chesneau, A. Ali Chérif, "Comparison of multicomponent fuel droplet vaporization experiments in forced convection with the Sirignano model," Experimental Thermal and Fluid Science 18 (1999) 282–290.
[2] G.M. Faeth, "Current status of droplet and liquid combustion," Prog. Energy Combust. Sci. 3 (1977) 191–224.
[3] C.K. Law, "Recent advances in droplet vaporization and combustion," Prog. Energy Combust. Sci. 8 (1982) 171–201.
[4] W.A. Sirignano, Theory of multi-component fuel droplet vaporization, Arch Thermodyn. Combust. 9 (2) (1978) 231–247.
[5] B. Abramzon, W.A. Sirignano, "Droplet vaporization model for spray combustion calculations," Int. J. Heat Mass Transfer 12 (9) (1989) 1605–1648.
[6] A. Berlemont, M.S. Grancher, G. Gouebet, "Heat and mass transfer coupling between vaporizing droplets and turbulence using a Lagrangian approach," Int. J. Heat Mass Transfer 38 (17) (1995) 3023–3034.
[7] M. Sommerfeld, H.H. Qiu, "Experimental studies of spray evaporation in turbulent flow," Int. J. Heat Fluid Flow 19 (1998) 10–22.
[8] J. Barata, "Modeling of bio-fuel droplets dispersion and evaporation," Renewable Energy 33 (4) (2008) 769–779.
[9] W.A. Sirignano, Fluid Dynamics and Transport of Droplets and Sprays, Cambridge University press, 1999.
[10] A. Saha, R. Kumar, and S. Basu, "Infrared thermography and numerical study of vaporization characteristics of pure and blended bio-fuel droplets," Int. J. Heat Mass Transfer 53 (19-20) (2010) 3862–3873.
[11] D.J. Torres, P.J. O'Rourke, A.A. Amsden, "Efficient multicomponent fuel algorithm," Combustion Theory and Modelling 7 (2003) 67-86.
[12] X. Gu, S. Basu, R. Kumar, "Dispersion and vaporization of biofuels and conventional fuels in a crossflow pre-mixer", Int. J. Heat Mass Transfer vol. 55, Issue 1-3, pp.336-346 (2012)
[13] P.J. O'Rourke, Collective drop effects on vaporizing liquid sprays, Ph.D. thesis, Princeton University, 1981.
[14] J. J. Nijdam , B. Guo, D.F. Fletcher and T. A. G. Langrish, Challenges of Simulating Droplet Coalescence within a Spray, Drying Technology, 22, (2004) 1463-1488.
[15] J. Qian, C.K. Law, Regimes of coalescence and separation in droplet collision, J. Fluid Mech., 331, pp. 59-80 (1997).
[16] Y.J. Jiang, A. Umemura, and C.K. Law, An experimental investigation on the collision behavior of hydrocarbon droplets, J. Fluid Mech., vol. 234, (1992). 171-190.
[17] S. Subramaniam, and P.J. O'Rourke, Numerical Convergence of the KIVA--3 code and its Implications for Modeling, Los Alamos Unclassified Report LAUR 98-5465 (1998).
[18] David P. Schmidt, C.J. Rutland, Reducing grid dependency in droplet collision modeling, J. Eng. Gas Turbines Power, Volume 126, Issue 2, (2004) 227-233.
[19] David P. Schmidt, C.J. Rutland, A new droplet collision algorithm, Journal of Computational Physics, Volume 164, Issue 1, pp. 62-80 (2000).
[20] A.A. Amsden, P.J. O'Rourke, and T.D. Bulter, "KIVA-II: A computer program for chemically reactive flows with sprays," Los Alamos National Laboratory, LA-11560-MS, 1989.
[21] T.L. Georjon, R. Reitz, A drop-shattering collision model for multidimensional spray computations, Atomization and Sprays, vol.9, pp.231-254 (1999).
[22] M. Renksizbulut, M.C. Yuen, Numerical study of droplet evaporation in a high temperature stream, J. Heat Transfer 105 (1983) 389–397.